analytical chemistry

Article

Cite This: *Anal. Chem.* 2020, 92, 1589−1597

pubs.acs.org/ac

Detection of Selenocysteine with a Ratiometric near-Infrared Fluorescent Probe in Cells and in Mice Thyroid Diseases Model

Xianzhu Luo,[†,‡] Rui Wang,[‡] Chuanzhu Lv,[‡] Guang Chen,[*,†] Jinmao You,[*,†] and Fabiao Yu[*,†,‡]

[†]The Key Laboratory of Life-Organic Analysis, Key Laboratory of Pharmaceutical Intermediates and Analysis of Natural Medicine, College of Chemistry and Chemical Engineering, Qufu Normal University, Qufu 273165, China

[‡]Institute of Functional Materials and Molecular Imaging, Key Laboratory of Emergency and Trauma, Ministry of Education, Key Laboratory of Hainan Trauma and Disaster Rescue, College of Clinical Medicine, College of Emergency and Trauma, Hainan Medical University, Haikou 571199, China

Supporting Information

ABSTRACT: The pathological progression of thyroid diseases poses a serious threat to human health. Because thyroid diseases are closely related to selenocysteine (Sec), it is necessary to investigate the relationship between Sec and thyroid diseases. Herein, we design and synthesize a ratiometric near-infrared fluorescent probe (Mito-Cy-Sec) to analyze the fluctuations and roles of Sec in cells and in mice thyroid diseases model. The probe is composed of a near-infrared heptamethine cyanine fluorophore, an acrylamide as the response moiety, and a lipophilic triphenylphosphonium cation as the mitochondrial localization group. After reacting with Sec for 5 min, the probe Mito-Cy-Sec exhibits a distinct ratiometric fluorescence signal accompanied by a color change from green to blue. The applicability of Mito-Cy-Sec in mitochondrial localization is assessed via the super-resolution imaging. Mito-Cy-Sec has been successfully applied to detect the fluctuations of Sec concentration in human thyroid epithelial/cancer cell lines (Nthy-ori-3 cells/BHT101 cells) and mice thyroid disease (thyroiditis and thyroid cancer) models. Besides, both of our probes Mito-Cy-Sec and commercial ROSGreen H_2O_2 are employed to examine the interrelationship between H_2O_2 and Sec in cells and in mice models. The results demonstrate that the relevant-levels between H_2O_2 and Sec are exactly negative correlation. The related-levels of Sec and H_2O_2 may be identified as diagnostic indicators for the auxiliary diagnosis of thyroid diseases. We suppose that our probe Mito-Cy-Sec can be employed as a promising chemical tool for the diagnosis of thyroid diseases.

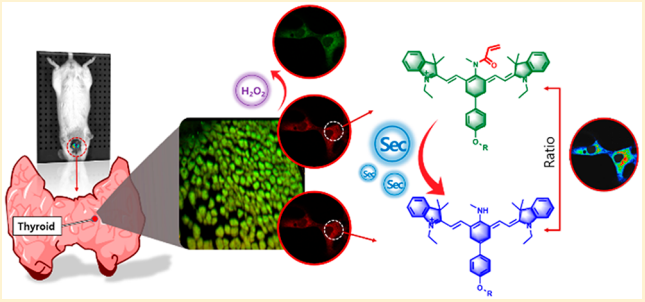

Thyroid cancer is one of the most common endocrine malignant tumors, and its morbidity is sustaining to increasing around the world.[1,2] In addition, other thyroid diseases also seriously threaten human health, such as thyroiditis. It is well-known that severe iodine deficiency can block the cellular synthesis and secretion of the thyroid hormone, which can result in a series of thyroid diseases.[3,4] Accumulating evidence shows that trace elements are necessary for thyroid hormone secretion, such as selenium (Se).[5] Selenocysteine (Sec) is the 21st natural amino acid and appears to be the main chemical form of Se present in living organisms.[6] In addition, Sec has been recognized as the active site of selenoproteins (Seps)-related enzymes, such as glutathione peroxidase (GPx) and thioredoxin reductase (TrxR), as well as iodothyronine deiodinase, which involve many significant physiological processes.[7−9] As is known, the abnormal levels of Sec possess an important relationship with several diseases, for instance, thyroid diseases, cardiovascular disease, diabetes, and neurodegenerative diseases.[10−12] The intracellular homeostasis between the reduction of GPx activity and the upregulation levels of hydrogen peroxide (H_2O_2) in a Sec-deficient state will lead to a local oxidative damage and will cause the occurrence of thyroid disease.[5,13−16]

Mitochondria are involved in many physiological processes whose functions are critical for maintaining the cellular redox homeostasis.[17,18] Although mitochondria exist at the antioxidant capacity, it is difficult to avoid oxidative damage induced by the suddenly excessive production of reactive oxygen species (ROS), such as H_2O_2.[19−21] Coincidentally, Sec processes the certain antioxidant capacity and dominates the mitochondrial oxidative damage raised by ROS.[22] Therefore, to understand the relationship between the Sec and H_2O_2 in thyroid diseases, it is necessary for us to develop a direct method to rapidly detect Sec in biological systems.

The current techniques for the detection of Sec include liquid chromatography,[23] nuclear magnetic resonance spectroscopy,[24] and capillary high performance liquid phase-inductively coupled plasma mass spectrometry (HPLC-

Received: October 24, 2019
Accepted: December 9, 2019
Published: December 9, 2019

DOI: 10.1021/acs.analchem.9b04860
Anal. Chem. 2020, 92, 1589−1597

MS).[25] Although these methods are accurate for the detection of Sec, they require cumbersome sample pretreatment and fail to monitor the changes of intracellular Sec in real-time and in situ.[26] With a comparison to the above analytical techniques, small molecule fluorescent probes have been performed as indispensable tools for the visualizing and imaging of biologically active species due to their high sensitivity, good selectivity, and noninvasiveness, as well as high spatial and temporal resolution.[27−31] However, there are still challenges for the detection of Sec in a living system owing to its high reactivity, instability, and chemical structure similar to other biothiols.[32,33] Several fluorescent probes are proposed for the analysis of Sec depending on different reaction mechanisms, including nucleophilic aromatic substitution reactions,[29,34] thiolysis of dinitrophenyl ether,[35] hydrolysis of acrylate,[36] and selenium−sulfur exchange reaction.[9] Although the entries have been elegantly constructed, the ratiometric near-infrared (NIR) fluorescent probe for intracellular Sec detection is rarely established.[9,26] The ratiometric NIR fluorescent probe is not only suitable for imaging in a living biological system because of its small photodamage to biological samples, strong penetrating ability, and low background,[37−43] but it is also capable of avoiding interference caused by uneven loading or distribution and environmental changes by spectral analysis at two different channels.[44−47] On the basis of these merits, we now strive to conceive a new ratiometric NIR fluorescent probe for the detection of Sec in living cells and in vivo.

Herein, to investigate the critical roles of Sec in thyroid diseases, we designed and synthesized a mitochondrial targeting ratiometric NIR fluorescent probe (Mito-Cy-Sec) that can sensitively detect the fluctuations of Sec in living cells and in a thyroid diseased mice model. The probe displayed a dual response of ratiometric fluorescence to Sec detection within 5 min without interference from other biothiols, such as cysteine (Cys). The probe Mito-Cy-Sec also could effectively target in mitochondria and sensitively detect the fluctuations of Sec concentration in living cells. Additionally, taking advantage of the conjunction of both Mito-Cy-Sec and commercial ROSGreen H_2O_2 probes, we verified the relationship between Sec and H_2O_2 in thyroiditis and thyroid cancer. Our experimental results indicate that the concentration association between Sec and H_2O_2 was a negative correlation in the two thyroid diseases. Furthermore, we evaluated the antioxidant and anti-inflammatory effects of intracellular Sec in cells and in the mice thyroid diseases model.

EXPERIMENTAL SECTION

Synthesis of Compound Mito-Cy-Sec. The compound Mito-Cy (99.7 mg, 0.1 mmol) and triethylamine (30 μL, 0.21 mmol) were added to a round-bottom flask containing 30 mL of tetrahydrofuran (THF) under an Ar atmosphere.[48] After the mixture was stirred at 0 °C for 30 min, acryloyl chloride (16.3 μL, 0.2 mmol) was added dropwise. The mixture was further stirred for 6 h at 25 °C under an Ar atmosphere. The solvent was removed under reduced pressure and the obtained residues were purified through a silica gel chromatography (200−300 mesh) with gradient eluent CH_2Cl_2 and CH_3OH (100:1 to 5:1, *v*/*v*). The compound Mito-Cy-Sec was obtained as blue solid (37.81 mg, yield: 36%). ^{1}H NMR (400 MHz, $CDCl_3$) δ (ppm): 8.34 (s, 1H), 7.80 (m, 9H), 7.71 (s, 7H), 7.59 (d, 2H), 7.38 (m, 6H), 7.26−7.15 (m, 2H), 7.09 (d, 2H), 6.56−6.44 (m, 2H), 6.33 (m, 1H), 6.22−6.06 (m, 2H), 5.74−5.61 (m, 1H), 4.72 (s, 2H), 4.18 (s, 4H), 3.67 (d, 2H), 3.35 (d, 3H), 2.99 (m, 3H), 2.74 (d, 2H), 2.38 (s, 2H), 1.65 (d,10H), 1.53 (d, 6H), 1.41 (s, 6H). ^{13}C NMR (100 MHz, $CDCl_3$), δ (ppm): 179.41, 175.34, 164.92, 156.90, 149.11, 148.81, 156.90, 149.11, 148.81, 139.42, 137.41, 136.21, 129.42, 129.06, 127.30, 126.30, 125.30, 125.15, 124.56, 123.12, 122.83, 121.25, 114.18, 112.84, 111.14, 101.86, 92.04, 72.40, 53.41, 49.82, 49.45, 43.36, 40.98, 34.59, 33.43, 32.41, 32.42, 28.69, 28.02, 25.39, 23.12, 18.62, 14.58, 13.43. HR-MS: *m*/*z* $C_{69}H_{75}N_6O_2P^{2+}$ calcd, 525.2839; found $[M]^{2+}$, 525.2834.

Establishment of Thyroid Diseases Cell Models. Nthy-ori3-1 cells and BHT 101 cells were cultured in F12K and DMEM medium containing 10% FBS and 1% antibiotics (penicillin/streptomycin, 100 U/mL) at 37 °C under a humidified atmosphere containing 5% CO_2. The chronic inflammation and acute inflammation were established by stimulation of pro-inflammatory cytokines (INF-γ) (100 ng·mL^{-1}) for 24 h and lipopolysaccharide (LPS; 1 μg·mL^{-1})/INF-γ (100 ng·mL^{-1}) for 6 h in Nthy-ori3-1 cells, respectively.

Establishment of Mice Thyroid Diseases Model. The porcine thyroglobulin (PTg) solution was thoroughly mixed with an equal volume of full Freund's adjuvant, and emulsified into a water-in-oil emulsion. Each BALB/c mouse was injected with 0.8 mg of the emulsion once a week for 2 times. After the third week, the water-in-oil emulsion of the incomplete Freund's adjuvant emulsified PTg was injected once per 2 weeks, three times in a row. The mice models of thyroiditis were successfully established after 8 weeks. Human thyroid ductal carcinoma cell line (TT cells) suspension (0.1 mL) was injected into BALC/c mice, and the thyroid cancer mice models were successfully established after 8 weeks. The therapy groups were pretreated with 500 μg·kg^{-1} selenocystine (intraperitoneal injection, i.p.) in saline daily for 8 weeks before inducing mice thyroid diseases model. All the mice models were treated with Mito-Cy-Sec (10 μM, 50 μL in DMSO/saline = 1:99, *v*/*v*) and ROSGreen H_2O_2 (5 μM, 50 μL in DMSO/saline = 1:99, *v*/*v*) for 30 min through neck injection before in vivo fluorescence imaging. TT cells (purchased from Shanghai Institute of Cell Biology, Chinese Academy of Sciences) were cultured in DMEM medium (Gibco) containing 10% fetal bovine serum in a 5% CO_2 incubator at 37 °C under saturated humidity.

RESULTS AND DISCUSSION

Design and Synthesis of Mito-Cy-Sec. The reasonable design of effective small molecule fluorescent probe is of great significance for achieving high specificity and selectivity.[43,45] The high reactivity, instability, and low biological concentration of Sec render it a huge challenging task to design Sec fluorescent probe without interference of other biothiols in living systems. It is worth noting that the pK_a of Sec is about 5.8, while the pK_a of the aliphatic thiol is around 8.5 (Cys, pK_a = 8.29 and GSH, pK_a = 8.75).[49−51] Under the neutral conditions, Sec is almost present as deprotonated anions, while biothiols exist as their protonated form, which suggests that Sec shows better nucleophilic capacity than other biothiols in a neutral environment.[9,52] Considering that the amide group is more stable than the ester group and is not easily hydrolyzed, we hypothesize that the acrylamide moiety can be potentially served as a desirable responsive-site for constructing a new type of fluorescent probe for the detection of Sec in living cells and in vivo. In addition, the introduction of acryloyl chloride into the meso-position of the heptamethine cyanine fluorophore will result in its NIR emission wavelength and

DOI: 10.1021/acs.analchem.9b04860
Anal. Chem. 2020, 92, 1589−1597

ratiometric characteristics, which can reduce certain light damage, increase tissue penetration and avoid the interference of the background signal.[9,26,53] Moreover, the meso-substitution may produce a large steric hindrance, which prevents the reaction with other Seps in cells. Owing to the negative membrane potential of the mitochondrial inner membrane, the cation compounds accumulate in the mitochondrial matrix. We choose a lipophilic triphenylphosphonium cation (PPh^{3+}) as the mitochondrial targeting moiety to guide our probe accumulating in mitochondria, because it can be commonly connected to interested bioactive molecules to improve its mitochondrial distribution.[54] As illustrated in Scheme 1, we

Scheme 1. Molecular Structure of Mito-Cy-Sec and Its Proposed Response Mechanism Towards Selenocysteine

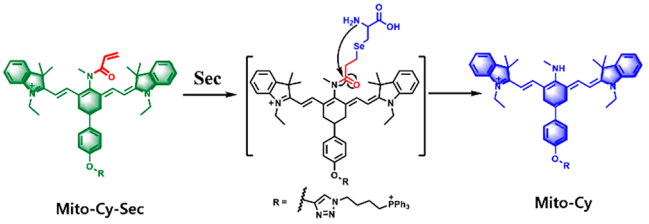

design and synthesize a new probe Mito-Cy-Sec for the detection of intracellular Sec. Our probe first proceeds the Michael addition reaction, then a nucleophilic reaction occurs, following the immediate cleavage of the amide bond, which triggers a large blue shift in emission wavelength based on intramolecular charge transfer (ICT) photophysical process.[55] Our desirable probe, Mito-Cy-Sec, exhibits sensitive and selective analysis of Sec in living cells and in vivo. The more information on the probe synthesis can be found in the Supporting Information.

Spectroscopic Properties. To evaluate the effectiveness of the probe Mito-Cy-Sec, the spectral properties of the probe versus Sec were tested under simulated physiological conditions (10 mM, HEPES, pH 7.4). As shown in Figure 1a, the probe behaved a strong absorption at 784 nm. After the addition of Sec, as expected, the maximum absorption wavelength blue-shifted to 623 nm. Meanwhile, the color of the testing solution changed from green to blue (Figure 1a, inset). Subsequently, we examined the fluorescence response of Mito-Cy-Sec to different concentrations of Sec. Correspondingly, there emerged a new fluorescence emission centered at 765 nm, while the maximum fluorescence emission at 825 nm sharply diminished (Figure 1b,c), which made it possible for the ratiometric detection of Sec. There obtained a good linear relationship between the logarithm of the ratio (F_{765nm}/F_{825nm}) and the Sec concentration from 0−15 μM (Figure 1d). The regression equation was $\lg(F_{765nm}/F_{825nm}) = 0.1312 \times [Sec] - 0.5359$, with $r = 0.9914$. Based on the standard method of $3\sigma/k$, the limit of detection was calculated as ~43 nM, and the experimental detection limit was detected as ~92 nM. The results indicated that the probe could be potentially severed as a new ratiometric NIR fluorescent probe for the quantitative and qualitative detection of Sec in cells.

Selectivity. High stability and selectivity in the physiological pH range are necessary for the new desirable fluorescent probes. Since Sec is rapidly metabolized and unstable in biological systems, the reaction kinetic of Mito-Cy-Sec on Sec has been studied in HEPES buffer solution (10 mM, pH 7.4). As shown in Figures 1e and S2, after the

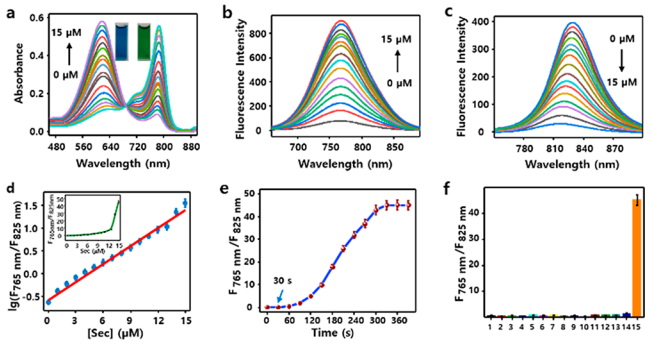

Figure 1. Spectral properties and selectivity of Mito-Cy-Sec. Data were recorded after 5 min incubated with different concentration of Sec (0−15 μM) at 37 °C in HEPES (pH 7.4, 10 mM). Dose-dependent absorbance spectra (a), emission spectra (b) (λ_{ex} = 630 nm, λ_{em} = 720−780 nm), and (c) (λ_{ex} = 730 nm, λ_{em} = 780−840 nm). (d) The linear relationship between $\lg(F_{765nm}/F_{825nm})$ and Sec. Inset: Ratiometric intensity changes with different concentrations of Sec. (e) Time-dependent fluorescent ratio (F_{765nm}/F_{825nm}) toward Sec during 0−390 s, and the probe was added at 30 s. (f) The fluorescent ratio (F_{765nm}/F_{825nm}) response of Mito-Cy-Sec to various reactive species at 5 min: 1, blank; 2, 150 μM GSH; 3, 150 μM Cys; 4, 150 μM Hcy; 5, 15 μM NaHS; 6, 15 μM NAC; 7, 15 μM selenomethionine; 8, 15 μM selenocystine; 9, 15 μM Se-methylselenocysteine; 10, 15 μM ascorbic acid; 11, 15 μM GPx; 12, 15 μM TrxR; 13, 15 μM Na_2SeO_3; 14, 15 μM DTT; 15, 15 μM Sec. The experiments were repeated three times and the data were shown as mean (±S.D.).

addition of Sec, the fluorescence ratiometric signal reached maximum within 5 min and remained stable during 4 h, which indicated that our probe could be utilized to real-time imaging of Sec in living cells. In addition, high selectivity is crucial to an excellent probe. We next investigated the response of Mito-Cy-Sec toward varies interfering analytes. As exhibited in Figure 1f, the addition of biothiols and Sec analogs (GSH; Cys; Hcy; NaHS; NAC; selenomethionine; $(Sec)_2$; Se-methyl selenocysteine; ascorbic acid; Gpx; TrxR; and Na_2SeO_3) hardly induced fluorescence ratiometric changes. It was delightful that biothiols, such as GSH, Cys, Hcy, TrxR, and Gpx, caused negligible ratiometric-fluorescence signal changes during 4 h (Figure S2).

We also assessed the fluorescence ratiometric signal toward other analytes, including reactive oxygen species (ROS), reactive nitrogen species (RNS), and anions and cations (Figure S3). The probe had no response to these interferences, which further confirmed that the probe Mito-Cy-Sec could be used to detect Sec. High-performance liquid phase (HPLC) experiments had been performed to further evaluate the selectivity of our probe toward Sec (Figure S4). The peak of Mito-Cy-Sec located at 3.76 min and a new peak at 4.52 min appeared after Sec was added. The major interfering species Cys only offered a quite inferior peak at 4.52 min. The results displayed that only Sec could selectively cleave the amide bond in the structure of Mito-Cy-Sec. We also estimated the impact of pH on Mito-Cy-Sec in the absence and presence of Sec. The fluorescence intensity of the probe Mito-Cy-Sec remained almost unchanged during pH range 4.0−8.0 (Figure S5). The results indicated that the probe could be applied to the detection of Sec in the living system.

Images of Exogenous and Endogenous Sec in Cells. To evaluate the capability of Mito-Cy-Sec to detect Sec in living cells, we performed Cells Counting Kit-8 (CCK-8) assay to assess cytotoxicity of the probe Mito-Cy-Sec against four

DOI: 10.1021/acs.analchem.9b04860
Anal. Chem. 2020, 92, 1589−1597

kinds of cells. The results clearly showed that our probe possessed low cytotoxicity in cells (Figure S6). Since the probe Mito-Cy-Sec had features of higher sensitivity, selectivity, and low cytotoxicity, the probe should be suitable for Sec detection in living cells. HeLa cells were selected as the testing cell models. As shown in Figure 2, all cells were incubated with

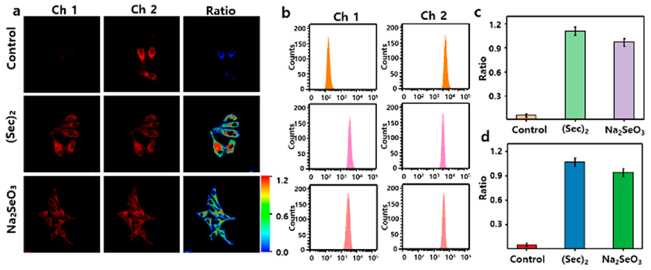

Figure 2. Fluorescence images and flow cytometry analyses of endogenous and exogenous Sec in Hela cells. (a) Incubated with Mito-Cy-Sec (10 μM) for 10 min as control. Another two cell groups were pretreated with $(Sec)_2$ (2 μM) and Na_2SeO_3 (5 μM) for 12 h, then incubated with 10 μM probe for 10 min, respectively. Fluorescence collection windows for Ch 1: 720−780 nm (λ_{ex} = 630 nm), Ch 2: 780−840 nm (λ_{ex} = 730 nm). (b) Corresponding flow cytometry analysis. (c) The average ratiometric values in (a). (d) Mean ratiometric values in (b). The experiments were repeated three times and the data were shown as mean (±S.D.).

Mito-Cy-Sec (10 μM) for 10 min, then fluorescence images were obtained utilizing a laser scanning confocal microscope. The ratiometric fluorescence images were reconstructed from two channels: Ch 1: λ_{ex} = 630 nm, λ_{em} = 720−780 nm, Ch 2: λ_{ex} = 730 nm, λ_{em} = 780−840 nm. The pseudocolor ratiometric images were presented to illustrate the intensity ratiometric in Ch 1 versus Ch 2. The control cells in Figure 2a were incubated with Mito-Cy-Sec (10 μM) for 10 min, weak fluorescence in Ch 1 and strong fluorescence in Ch 2 indicated that the probe displayed significant inertness to other intracellular species in living cells, such as biothiols. Intracellular Sec could be produced by the reaction of exogenous $(Sec)_2$ with intracellular biothiols.[33,36] After pretreating with $(Sec)_2$ for 12 h, the HeLa cells were subsequently incubated with Mito-Cy-Sec (10 μM) for imaging of Sec. As expected, the fluorescence intensity increased in Ch 1 and significantly decreased in Ch 2 along the extension of time points at 1, 3, 6, and 12 h (Figures 2 and S7). The cells provided time-dependent ratiometric fluorescence images, which implied the increasing Sec concentrations in HeLa cells. We further tested the possibility of Mito-Cy-Sec tracking endogenous Sec in HeLa cells. Na_2SeO_3 can induce the increase of endogenous Sec levels in living cells through a succession of physiological processes.[11,56] As shown in Figures 2a and S8, there appeared a strong fluorescence signal in Ch 1 after stimulation with Na_2SeO_3 for 12 h, while the distinctly reduced fluorescence signal in Ch 2 could be observed. The concentration of Sec was finally estimated as 3.92 ± 0.15 and 3.41 ± 0.13 μM when cells were incubated with 2 μM $(Sec)_2$ and 5 μM Na_2SeO_3 for 12 h, respectively. Flow cytometry analysis was employed to further verify our obtained data (Figure 2b,d). The analysis results were well consistent with ratiometric fluorescence images (Figure 2a,b). All these results demonstrated that this probe was suitable for imaging of endogenous and exogenous Sec in living cells.

Mitochondrial Localization. Mitochondria are involved in a number of key physiological activities in cells.[18] Monitoring the level changes of Sec in mitochondria can promote the better comprehension of its biofunction during a certain biological event. We further checked the mitochondrial localization capability of the probe Mito-Cy-Sec. Co-staining experiment was performed in HepG2 cells. Two commercial mitochondrial dyes (Mito Tracker Green FM dye and Rhodamine 123 dye) were employed to assess whether the probe Mito-Cy-Sec could specifically accumulate in mitochondria or not. The color pairs of each pixel of Rhodamine 123 and Mito-Cy-Sec channels displayed a high correlated plot (Figure S9). Pearson's colocalization coefficient was determined as R_r = 0.97. Subsequently, we investigated the applicability of Mito-Cy-Sec in mitochondrial localization via the super-resolution imaging.

The cells were stained with Mito Tracker Green FM and Mito-Cy-Sec (Figure 3b,c), respectively. With comparison of

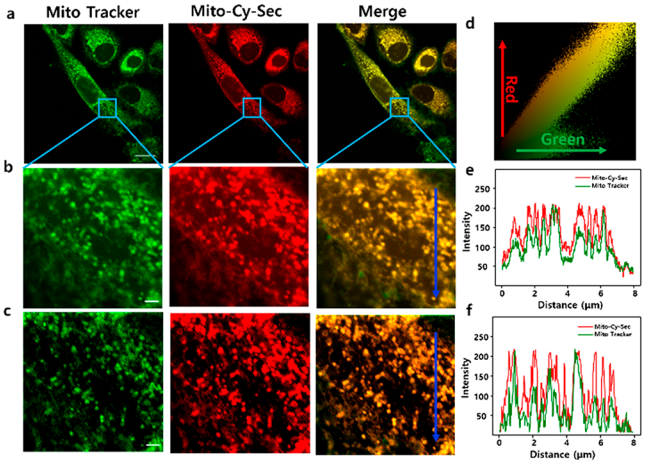

Figure 3. Mitochondrial colocalization with Mito-Cy-Sec and Mito Tracker Green FM in HepG2 cells. Fluorescence collection windows for green channel: 500−550 nm (λ_{ex} = 488 nm), and red channel: 780−840 nm (λ_{ex} = 730 nm). (a) Cells were stained with MitoTracker Green FM (200 nM) for 30 min and Mito-Cy-Sec (10 μM) for 10 min, scale bar: 10 μm. (b) Enlarged images in the field view of the cyan frame in (a) for mitochondrial colocalization. (c) Super-resolution imaging of mitochondria with the same region in (b), scale bar: 2 μm. (d) The colocalization and correlation between the selected red and green channels in (a). (e, f) Intensity profile of the blue arrow in (b) and (c) across cell, respectively.

the images obtained from laser scanning confocal microscopy, the super-resolution imaging provided clearer mitochondrial localization images, which indicated that Mito-Cy-Sec could dominantly accumulate in mitochondria rather than other organelles. The multicolor colocalization showed a high correlation plot (Figure 3d) and the Pearsons's coefficient was Rr = 0.96, the Manders' coefficients were m_1 = 0.99 and m_2 = 0.98. The intensity profile of the blue arrows across the HepG2 cells were completely synchronous. But the super-resolution images exhibited more accurate plot (Figure 3e,f). All these results demonstrated the specific mitochondrial localization of Mito-Cy-Sec in living cells.

Detection of Intracellular Sec in Real-Time. A series of evidence confirm that thyroid diseases are associated with the levels of intracellular Sec.[5,57] However, the pathogenic mechanisms of thyroid diseases are not clear yet.[6] Therefore,

DOI: 10.1021/acs.analchem.9b04860
Anal. Chem. 2020, 92, 1589−1597

to understand the relationship between Sec and thyroid diseases, it is necessary to investigate the concentration fluctuations of intracellular Sec. Nthy-ori3-1 cells and BHT101 cells were selected as the testing cell models. As shown in Figure 4a, the ratiometric signals increased along

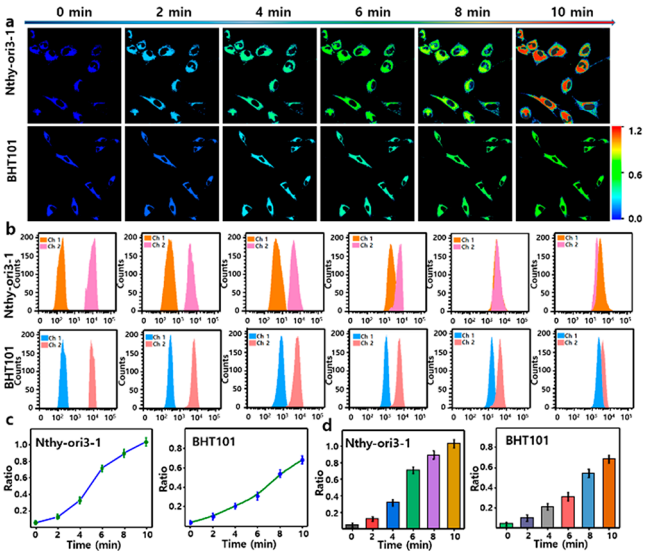

Figure 4. Imaging of endogenous Sec in Nthy-ori3-1 and BHT101 cells. (a) Pseudocolor ratiometric images of endogenous Sec generation in Nthy-ori3-1 cells and BHT101 cells at different time points: 0, 2, 4, 6, 8, and 10 min. (b) Flow cytometry analysis for (a). (c, d) Average ratiometric intensities changes of Mito-Cy-Sec toward Nthy-ori3-1 and BHT101 cells in (a) and (b), respectively. The experiments were repeated three times and the data were shown as mean (±S.D.).

with the extension of incubation time (0−10 min) in Nthy-ori3-1 and BHT101 cells. However, the ratiometric signals of the two cells displayed significant discrimination at 10 min, indicating that the Sec levels were different in various types of cell lines. The mean ratiometric values at 10 min were 1.02 and 0.68, and the Sec concentrations were estimated to be 3.48 ± 0.15 μM and 2.33 ± 0.11 μM, respectively. To verify the accuracy quantitative analysis of the probe, HPLC analysis was further performed to quantify Sec derivatized by iodoacetamide.[9] The HPLC analysis results were 3.64 ± 0.16 and 2.52 ± 0.13 μM in Nthy-ori3-1 and BHT101 cells, respectively (Figure S11 and Table S1). The corresponding flow cytometry analysis was performed (Figure 4b,d). The obtained results were well consistent with the ratiometric imaging (Figure 4c). All experiment results revealed that the probe Mito-Cy-Sec could be used to real-time detect Sec in living cells.

Images of Sec in Different Types of Thyroid Diseases Cells Model. The occurrence of diverse thyroid diseases is frequently associated with the level of H_2O_2.[58] Owing to the outstanding antioxidant and anti-inflammatory effects of Sec in cells, we supposed that Sec might suppress the burst of H_2O_2 and maintain the intracellular redox homeostasis during the occurrence and progression of thyroid diseases. Herein, in order to verify this hypothesis, the probe Mito-Cy-Sec and commercial ROSGreen H_2O_2 probe were used to reveal the relationship between intracellular Sec and H_2O_2 in the different thyroid diseases cell models, respectively. The pro-inflammatory cytokines INF-γ and lipopolysaccharide (LPS) are utilized to induce inflammation, which may promote the consumption of Sec.[55] We performed seven parallel experiments using different models of thyroid disease. All cells were incubated with the probe Mito- Cy-Sec (10 μM) at 37 °C for 10 min before imaging. Human thyroid epithelial cell line was selected as the control group (Nthy-ori3-1 cells, group a). Nthy-ori3-1 cells were pretreated with INF-γ (100 ng·mL^{-1}) for 24 h to induce chronic inflammation as group b. Nthy-ori3-1 cells in group c were treated with LPS (1 μg·mL^{-1})/INF-γ (100 ng·mL^{-1}) for 6 h, inducing acute inflammation. Human thyroid cancer cell line (BHT 101 cells) was chosen as group d. $(Sec)_2$ can be converted to Sec in cells, which prevents and treats inflammation and other oxidative stress related diseases, thus, it can be considered as the direct source of Sec.[11,31] The Nthy-ori3-1 cells were incubated with 50 μM $(Sec)_2$ for 2 h and then stimulated by INF-γ (100 ng·mL^{-1}) and LPS (1 μg·mL^{-1})/INF-γ (100 ng·mL^{-1}) as groups e and f, respectively. The BHT101 cells of group g were incubated with 50 μM $(Sec)_2$ for 2 h.

Cells in group a provided powerful ratiometric signals, revealing higher levels of Sec in Nthy-ori3-1 cells. Group b displayed a higher ratiometric signal than group c. The ratiometric signal of group d was faint. The results revealed that the levels of Sec were different in diverse thyroid diseases. The fluorescence signals were sorted as group a > group b > group c > group d. The results illustrated that the more serious the thyroid disease the lower the concentration of Sec. Fluorescence ratiometric signals of group e and group f were stronger than group b and group c, respectively, which was benefit from the higher level of Sec. However, the ratiometric signals of group f and group g were almost the same. Meanwhile, we also assessed the level changes of H_2O_2 (Ch 3) in these cell models. As illustrated in Figure 5a, c, and d, the levels between H_2O_2 and Sec were exactly negative correlation. According to the ratio values of these images, the levels of Sec were arranged from highest to lowest in an order of group a > group e > group f > group b > group c > group d ≈ group g. The results demonstrated that Nthy-ori3-1 cells stimulated by INF-γ or LPS/INF-γ could result in varying degrees of inflammation and could lead to different degrees of H_2O_2 burst in cells. We employed flow cytometry analysis to further verify the above results. The flow cytometry analysis and fluorescence ratiometric signal were basically consistent with each other. The disturbance of redox homeostasis inevitably causes cell apoptosis. The apoptosis rates of these seven testing groups were further assessed via Annexin V-FITC/propidium iodide (PI) assay. The apoptosis and necrosis rates were ordered as group c > group b > group f > group e > group a ≈ group d ≈ group g (Figure 5g). The results clearly revealed that intracellular Sec processed certain anti-inflammatory and protective abilities to living cells. The results suggested that the probe could effectively analyze the fluctuation of Sec in different thyroid disease cell models. Moreover, the levels of Sec and H_2O_2 might be identify as diagnostic indicators for the assistant of thyroid diseases diagnosis.

Imaging of Sec in Mice Thyroid Diseases Model. We next assessed the capability of Mito-Cy-Sec for the detection of Sec in vivo. The BALB/c mice were selected as experimental animal models. For evaluating the fluctuation and protective effects of Sec in thyroid diseases, the mice models were divided into five groups: group a was the control group (normal mice); group b was the thyroiditis group; group c was the thyroid cancer group. The therapy groups of thyroiditis (group d) and thyroid cancer (group e) were pretreated with 500 μg·kg^{-1}

DOI: 10.1021/acs.analchem.9b04860
Anal. Chem. 2020, 92, 1589−1597

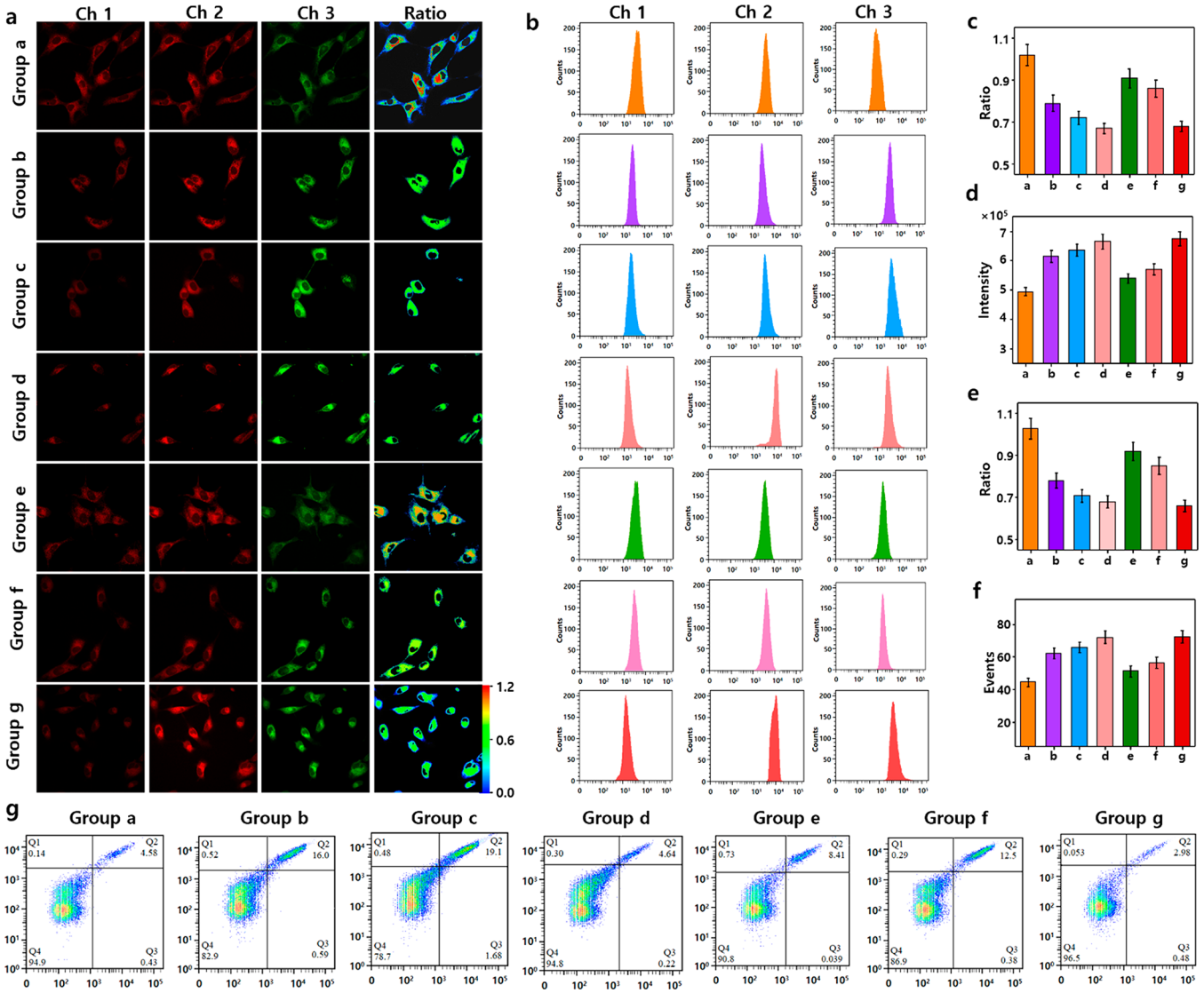

Figure 5. Ratiometric fluorescence images of Sec in different types of thyroid disease cell models with Mito-Cy-Sec (10 μM) and ROSGreen H_2O_2 (5 μM) by confocal microscopic imaging and flow cytometry analysis. (a) The ratiometric images of endogenous Sec in thyroid model cells. Group a: Nthy-ori3-1 cells; Group b: Nthy-ori3-1 cells stimulated by INF-γ for 24 h; Group c: Nthy-ori3-1 cells stimulated by INF-γ/LPS for 6 h; Group d: BHT101 cells; Group e: Nthy-ori3-1 cells incubated with 50 μM selenocysteine $(Sec)_2$ for 2 h before stimulated by INF-γ; Group f: Nthy-ori3-1 cells incubated with 50 μM $(Sec)_2$ for 2 h before stimulated by INF-γ/LPS; and Group g: BHT101 cells incubated with 50 μM $(Sec)_2$ for 2 h. Fluorescence collection windows for Ch 1: 720−780 nm (λ_{ex} = 630 nm), Ch 2: 780−840 nm (λ_{ex} = 730 nm), and Ch 3: 500−550 nm (λ_{ex} = 488 nm). (b) Flow cytometry analysis of the cells in (a). (c) The average ratio (Ch 1/Ch 2) values in (a). (d) Mean fluorescent intensities of Ch 3 in (a). (e) The average ratio (Ch 1/Ch 2) values in (b). (f) Mean fluorescent intensities of Ch 3 in (b). (g) Apoptosis and necrosis assays of groups a−g in (a) by Annexin V-FITC/propidium iodide (PI). Q1, necrosis; Q2, late apoptosis; Q3, early apoptosis; Q4, viable. Scale bar: 20 μm. The experiments were repeated three times and the data were shown as mean (±S.D.).

$(Sec)_2$ (i.p.) in saline daily for 8 weeks before the same performance as group b and group c, respectively. To determine whether the mice thyroid diseases model was successfully established or not (Figure 6b,c), hematoxylin-eosin (H&E), and Masson staining were utilized to illustrate the pathological morphology of the thyroid. Group a exhibited complete thyroid follicles and regular morphology. The follicular cavity contained a medium amount of pink jelly, the rich filter interstitial capillaries, and no lymphocyte immersion. The tissue of group b mice offered the expanded thyroid follicles, and the filter cavity was filled with a great deal of pink jelly. The part of the visible follicle structure foam was poor, and the filter was observed among small focal lymphocyte immersions. Tumors in Group c grew vigorously, and provided only a few residual follicular structures. There existed varying degrees of tracheal infiltration and tracheal cartilage destruction. The above results clearly indicated that the mice models were successfully established.

All the BALB/c mice were treated with Mito-Cy-Sec (10 μM, 50 μL in DMSO/saline = 1:99, v/v) and ROSGreen H_2O_2 (5 μM, 50 μL in DMSO/saline = 1:99, v/v) for 30 min through neck injection before in vivo fluorescence imaging. The representative fluorescence images (pseudocolor) were shown in Figure 6a; meanwhile, the corresponding mean ratio values were listed in Figure 6e. The ratio values of group a were significantly higher than those of groups b and c. The ratiometric fluorescence signals from strong to weak was sorted in an order: group a > group b > group c, which displayed that

DOI: 10.1021/acs.analchem.9b04860
Anal. Chem. 2020, 92, 1589−1597

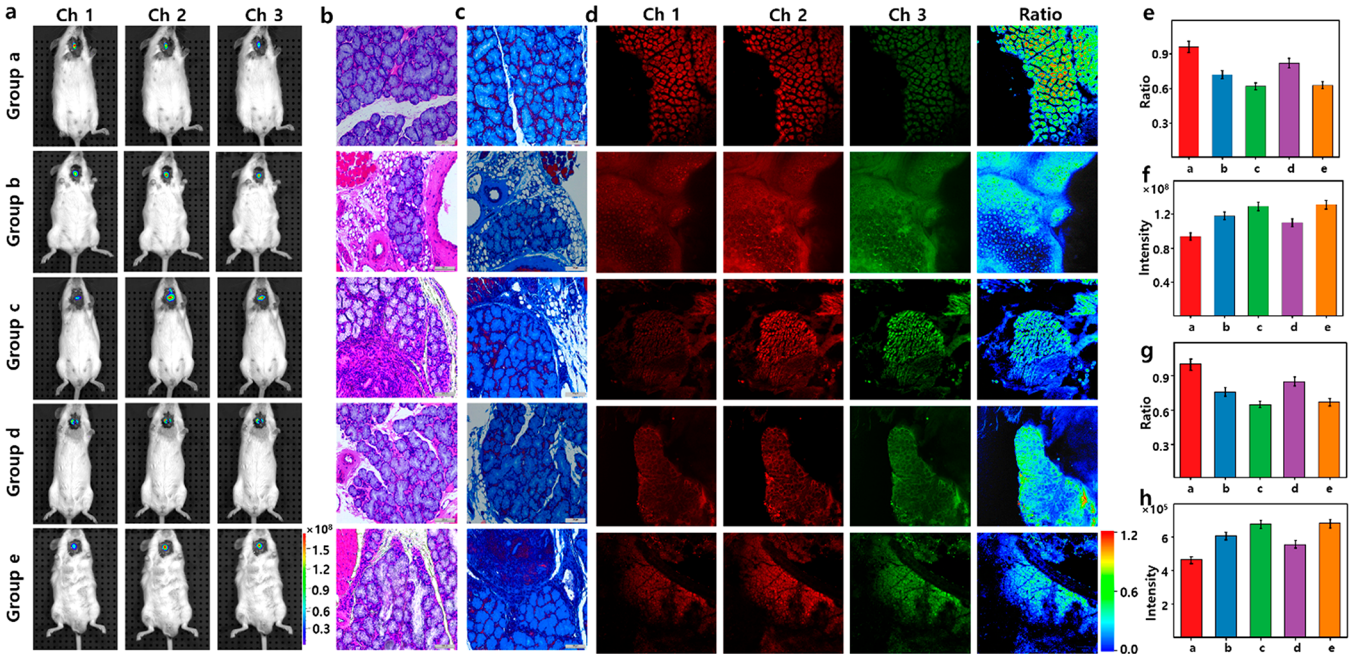

Figure 6. In vivo imaging of Sec in different mice thyroid diseases model. (a) Fluorescence images of mice in groups a−e; group a, control group; group b, thyroiditis mice group; group c, thyroid cancer mice; group d, BALB/c mice were pretreated with 500 $\mu g \cdot kg^{-1}$ selenocystine (intraperitoneal injection, (i.p.)) in saline daily for 8 weeks before the same treatment of group b; and group e, BALB/c mice were pretreated with 500 $\mu g \cdot kg^{-1}$ selenocystine (i.p.) in saline daily for 8 weeks before the same treatment as group c. All the mice models were treated with Mito-Cy-Sec (10 μM, 50 μL in DMSO/saline = 1:99, *v*/*v*) and ROSGreen H_2O_2 (5 μM, 50 μL in DMSO/saline = 1:99, *v*/*v*) for 30 min through neck injection before in vivo fluorescence imaging. Fluorescence collection windows for Ch 1: 720−780 nm (λ_{ex} = 630 nm), Ch 2: 780−840 nm (λ_{ex} = 730 nm), Ch 3: 500−550 nm (λ_{ex} = 488 nm), and ratio: Ch 1 versus Ch 2. (b) H&E stained thyroid tissues histopathology images. (c) Masson's stained slices of thyroid tissues. (d) Fluorescence images of different fresh mice thyroid diseases slices by simultaneously incubated with Mito-Cy-Sec (10 μM) and ROSGreen H_2O_2 (5 μM) for 20 min. (e) The average ratio (Ch 1 vs Ch 2) values in (a). (f) Mean fluorescent intensities of Ch 3 in (a). (g) The average ratio (Ch 1 vs Ch 2) values in (d). (h) Mean fluorescent intensities of Ch 3 in (d).

the concentration of Sec varied in different thyroid diseases. The level fluctuations of H_2O_2 in these models were measured simultaneously. The fluorescence signals were sorted as group c > group b > group a (Figure 6f). The results demonstrated that the relevant-levels between H_2O_2 and Sec were precisely negative correlation in these established models, which was well consistent with the results in the cell models (Figure 5). Therefore, the related level changes between H_2O_2 and Sec might be employed as an auxiliary method for thyroid diseases diagnosis. Compared with group b, the ratiometric signal of group d was stronger. H&E slices in Figure 6b also showed that the progression of inflammation in group d was lower than that of group b. The phenomenon was beneficial from the anti-inflammatory and protective effects of intracellular Sec. The ratiometric fluorescence signals and the pathological results of groups c and e were almost the same, indicating that Sec could not evidently alleviate the symptoms of cancer.

To directly confirm the level changes of Sec in vivo, fresh mice slices were prepared utilizing vibration slicer. The fluctuations of ratiometric fluorescence signals (Figure 6d) were consistent with the results in Figure 6a. To highlight the imaging depth of the probe Mito-Cy-Sec, we performed axial plane reconstruction of the three-dimensional (3D) image (Figure 7). The probe could be fully penetrated and imaged in tissues of 200 μm thickness. The above results revealed that the probe possessed good penetration ability and could be used for Sec imaging in different types of mice thyroid diseases. Although the mechanism of Sec roles was unclear, the abnormal levels of the Sec could lead to thyroid diseases, which was verified by more and more evidence. The relevant-levels of Sec and H_2O_2 in thyroid might be served as diagnostic indicators for the auxiliary diagnosis of thyroid diseases.

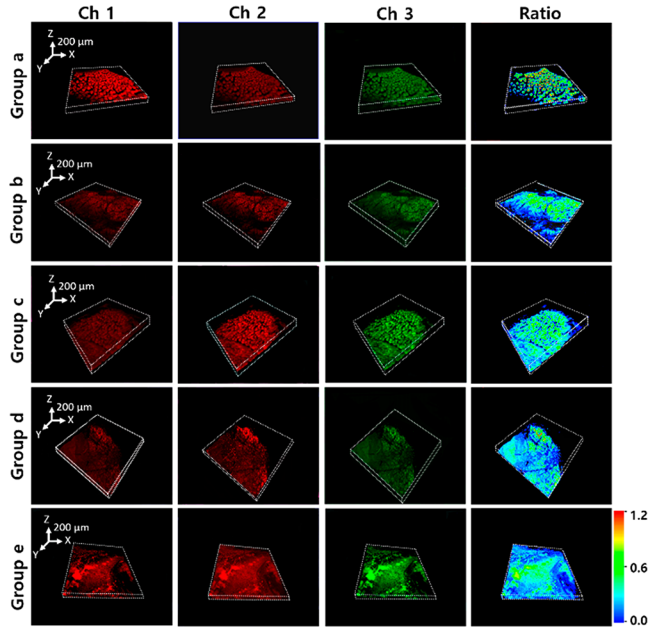

Figure 7. Fluorescence 3D images of different mice thyroid diseases slices incubated with Mito-Cy-Sec (10 μM) and ROSGreen H_2O_2 (5 μM) for 20 min. Fluorescence collection windows for Ch 1: 720−780 nm (λ_{ex} = 630 nm), Ch 2: 780−840 nm (λ_{ex} = 730 nm), Ch 3: 500−550 nm (λ_{ex} = 488 nm), and ratio images: Ch 1/Ch 2.

DOI: 10.1021/acs.analchem.9b04860
Anal. Chem. 2020, 92, 1589−1597

CONCLUSION

In summary, we develop a mitochondrial-targeting ratiometric NIR fluorescent probe (Mito-Cy-Sec) for the detection of Sec in living cells and in vivo. Mito-Cy-Sec not only detects the fluctuations of intracellular Sec in real-time, but also avoids interference with the high levels of biothiols under physiological conditions. The lipophilic triphenylphosphonium cation can guide the probe dominant accumulation in mitochondria, which is verified utilizing super-resolution imaging. Furthermore, this probe has been applied in conjunction with a commercial ROSGreen H_2O_2 probe to investigate the relationship between Sec and H_2O_2 in cells and in different mice thyroid disease models. The levels of Sec and H_2O_2 are exactly negative correlation in thyroid diseases. The results further confirm that endogenous Sec processes certain anti-inflammatory and protective effects. We hope that the probe Mito-Cy-Sec can serve as a potential chemical tool for the diagnosis of thyroid diseases.

ASSOCIATED CONTENT

Supporting Information

The Supporting Information is available free of charge at https://pubs.acs.org/doi/10.1021/acs.analchem.9b04860.

More experimental materials and details, synthesis steps, and compounds characterization (PDF)

AUTHOR INFORMATION

Corresponding Authors

*E-mail: fbyu@yic.ac.cn.
*E-mail: jmyou6304@163.com.
*E-mail: chenandguang@163.com.

ORCID

Guang Chen: 0000-0002-0454-1686
Fabiao Yu: 0000-0003-0073-6299

Notes

The authors declare no competing financial interest.

ACKNOWLEDGMENTS

This work was supported by the Hainan Provincial Higher Education Research Project (Hnky2019ZD-30), National Natural Science Foundation of China (Nos. 21864011 and 21775162), Research Unit of Island Emergency Medicine, Chinese Academy of Medical Sciences (Grant No. 2019RU013), Talent Program of Hainan Medical University (Grant Nos. XRC180006 and XRC180007), and Hundred Talent Program of Hainan (2018).

REFERENCES

(1) Nikiforov, Y. E.; Nikiforova, M. N. *Nat. Rev. Endocrinol.* **2011**, *7*, 569−580.
(2) Rahib, L.; Smith, B. D.; Aizenberg, R.; Rosenzweig, A. B.; Fleshman, J. M.; Matrisian, L. M. *Cancer Res.* **2014**, *74*, 2913−2921.
(3) Zimmermann, M. B.; Boelaert, K. *Lancet Diabetes Endocrinol.* **2015**, *3*, 286−295.
(4) Markou, K.; Georgopoulos, N.; Kyriazopoulou, V.; Vagenakis, A. G. *Thyroid* **2001**, *11*, 501−510.
(5) Schomburg, L.; Kohrle, J. *Mol. Nutr. Food Res.* **2008**, *52*, 1235−1246.
(6) Johansson, L.; Gafvelin, G.; Arner, E. S. *Biochim. Biophys. Acta, Gen. Subj.* **2005**, *1726*, 1−13.
(7) Wu, D.; Chen, L.; Kwon, N.; Yoon, J. *Chem.* **2016**, *1*, 674−698.
(8) Saito, Y.; Hayashi, T.; Tanaka, A.; Watanabe, Y.; Suzuki, M.; Saito, E.; Takahashi, K. *J. Biol. Chem.* **1999**, *274*, 2866−2871.
(9) Han, X.; Song, X.; Yu, F.; Chen, L. *Adv. Funct. Mater.* **2017**, *27*, 1700769.
(10) Weekley, C. M.; Harris, H. H. *Chem. Soc. Rev.* **2013**, *42*, 8870−8894.
(11) Brown, K. M.; Arthur, J. R. *Public Health Nutrition.* **2001**, *4*, 593−599.
(12) Kryukov, G. V.; Castellano, S.; Novoselov, S. V.; Lobanov, A. V.; Zehtab, O.; Guigo, R.; Gladyshev, V. N. *Science* **2003**, *300*, 1439−1443.
(13) Zhang, W.; Liu, T.; Huo, F.; Ning, P.; Meng, X.; Yin, C. *Anal. Chem.* **2017**, *89*, 8079−8083.
(14) Mehdi, Y.; Hornick, J. L.; Istasse, L.; Dufrasne, I. *Molecules* **2013**, *18*, 3292−2311.
(15) Sun, X.; Xu, S. Y.; Flower, S. E.; Fossey, J. S.; Qian, X.; James, T. D. *Chem. Commun.* **2013**, *49*, 8311−8414.
(16) Niethammer, P.; Grabher, C.; Look, A. T.; Mitchison, T. J. *Nature* **2009**, *459*, 996−999.
(17) Zhang, J.; Wang, Q.; Guo, Z.; Zhang, S.; Yan, C.; Tian, H.; Zhu, W. H. *Adv. Funct. Mater.* **2019**, *29*, 1808153.
(18) Li, X.; Hu, Y.; Li, X.; Ma, H. *Anal. Chem.* **2019**, *91*, 11409−11416.
(19) Lopez-Armada, M. J.; Riveiro-Naveira, R. R.; Vaamonde-Garcia, C.; Valcarcel-Ares, M. N. *Mitochondrion* **2013**, *13*, 106−118.
(20) Gao, M.; Wang, R.; Yu, F.; Chen, L. *Biomaterials* **2018**, *160*, 1−14.
(21) Sun, X.; Xu, Q.; Kim, G.; Flower, S. E.; Lowe, J. P.; Yoon, J.; Fossey, J. S.; Qian, X.; Bull, S. D.; James, T. D. *Chem. Sci.* **2014**, *5*, 3368−3373.
(22) Schmidt, R. L.; Simonovic, M. S. *Croat. Med. J.* **2012**, *53*, 535−550.
(23) Killa, H. M. A.; Rabenstein, D. L. *Anal. Chem.* **1988**, *60*, 2283−2287.
(24) Rabenstein, D. L.; Reid, R. S.; Yamashita, G.; Tan, K. S.; Arnold, A. P. *Anal. Chem.* **1986**, *58*, 1266−1269.
(25) Encinar, J. R.; Schaumlöffel, D.; Ogra, Y.; Lobinski, R. *Anal. Chem.* **2004**, *76*, 6635−6642.
(26) Han, X.; Wang, R.; Song, X.; Yu, F.; Chen, L. *Anal. Chem.* **2018**, *90*, 8108−8115.
(27) Tian, X.; Li, Z.; Sun, Y.; Wang, P.; Ma, H. *Anal. Chem.* **2018**, *90*, 13759−13766.
(28) Zhang, J. F.; Zhou, Y.; Yoon, J.; Kim, J. S. *Chem. Soc. Rev.* **2011**, *40*, 3416−3429.
(29) Wu, D.; Sedgwick, A. C.; Gunnlaugsson, T.; Akkaya, E. U.; Yoon, J.; James, T. D. *Chem. Soc. Rev.* **2017**, *46*, 7105−7123.
(30) Zhang, J.; Chai, X.; He, X. P.; Kim, H. J.; Yoon, J.; Tian, H. *Chem. Soc. Rev.* **2019**, *48*, 683−722.
(31) Li, X.; Gao, X.; Shi, W.; Ma, H. *Chem. Rev.* **2014**, *114*, 590−659.
(32) Chen, H.; Dong, B.; Tang, Y.; Lin, W. *Chem. - Eur. J.* **2015**, *21*, 11696−11700.
(33) Feng, W.; Li, M.; Sun, Y.; Feng, G. *Anal. Chem.* **2017**, *89*, 6106−6112.
(34) Zhang, B.; Ge, C.; Yao, J.; Liu, Y.; Xie, H.; Fang, J. *J. Am. Chem. Soc.* **2015**, *137*, 757−769.
(35) Li, M.; Feng, W.; Zhai, Q.; Feng, G. *Biosens. Bioelectron.* **2017**, *87*, 894−900.
(36) Tian, Y.; Xin, F.; Gao, C.; Jing, J.; Zhang, X. R. *J. Mater. Chem. B* **2017**, *5*, 6890−6896.
(37) Ou-Yang, J.; Li, Y.; Jiang, W. L.; He, S. Y.; Liu, H. W.; Li, C. Y. *Anal. Chem.* **2019**, *91*, 1056−1063.
(38) Zhou, D. Y.; Li, Y.; Jiang, W. L.; Tian, Y.; Fei, J.; Li, C. Y. *Chem. Commun.* **2018**, *54*, 11590−11593.
(39) Liu, H. W.; Hu, X. X.; Li, K.; Liu, Y.; Rong, Q.; Zhu, L.; Yuan, L.; Qu, F. L.; Zhang, X. B.; Tan, W. *Chem. Sci.* **2017**, *8*, 7689−7695.
(40) Guo, Z.; Park, S.; Yoon, J.; Shin, I. *Chem. Soc. Rev.* **2014**, *43*, 16−29.

DOI: 10.1021/acs.analchem.9b04860
Anal. Chem. 2020, 92, 1589−1597

(41) Yu, F.; Gao, M.; Li, M.; Chen, L. *Biomaterials* **2015**, *63*, 93−101.
(42) He, X.; Li, L.; Fang, Y.; Shi, W.; Li, X.; Ma, H. *Chem. Sci.* **2017**, *8*, 3479−3483.
(43) Yuan, L.; Lin, W.; Zheng, K.; He, L.; Huang, W. *Chem. Soc. Rev.* **2013**, *42*, 622−661.
(44) Zhang, J. F.; Zhou, Y.; Yoon, J.; Kim, Y.; Kim, S. J.; Kim, J. S. *Org. Lett.* **2010**, *12*, 3852−3855.
(45) Lee, M. H.; Kim, J. S.; Sessler, J. L. *Chem. Soc. Rev.* **2015**, *44*, 4185−4191.
(46) Wang, R.; Han, X.; You, J.; Yu, F.; Chen, L. *Anal. Chem.* **2018**, *90*, 4054−4061.
(47) Zhu, X.; Yuan, L.; Hu, X.; Zhang, L.; Liang, Y.; He, S.; Zhang, X.-B.; Tan, W. *Sens. Actuators, B* **2018**, *259*, 219−225.
(48) Sun, Y.; Yan, X.; Yuan, T.; Liang, J.; Fan, Y.; Gu, Z.; Zhang, X. *Biomaterials* **2010**, *31*, 7124−7131.
(49) Huber, R. E.; Criddle, R. S. *Arch. Biochem. Biophys.* **1967**, *122*, 164−173.
(50) Jung, H. S.; Chen, X.; Kim, J. S.; Yoon, J. *Chem. Soc. Rev.* **2013**, *42*, 6019−6031.
(51) Yue, Y.; Huo, F.; Cheng, F.; Zhu, X.; Mafireyi, T.; Strongin, R. M.; Yin, C. *Chem. Soc. Rev.* **2019**, *48*, 4155−4177.
(52) Nauser, T.; Dockheer, S.; Kissner, R.; Koppenol, W. H. *Biochemistry* **2006**, *45*, 6038−6043.
(53) Guo, Z.; Nam, S.; Park, S.; Yoon, J. *Chem. Sci.* **2012**, *3*, 2760−2765.
(54) Zielonka, J.; Joseph, J.; Sikora, A.; Hardy, M.; Ouari, O.; Vasquez-Vivar, J.; Cheng, G.; Lopez, M.; Kalyanaraman, B. *Chem. Rev.* **2017**, *117*, 10043−10120.
(55) Peng, X.; Song, F.; Lu, E.; Wang, Y.; Zhou, W.; Fan, J.; Gao, Y. *J. Am. Chem. Soc.* **2005**, *127*, 4170−4171.
(56) Areti, S.; Verma, S. K.; Bellare, J.; Rao, C. P. *Anal. Chem.* **2016**, *88*, 7259−7267.
(57) Zaichick, V. Y.; Tsyb, A. F.; Vtyurin, B. M. *Analyst* **1995**, *120*, 817−821.
(58) Hesse-Bähr, K.; Dreher, I.; Körle, J. *BioFactors* **2000**, *11*, 83−85.

DOI: 10.1021/acs.analchem.9b04860
Anal. Chem. 2020, 92, 1589−1597